NJC

New Journal of Chemistry

A journal for new directions in chemistry

Accepted Manuscript

This article can be cited before page numbers have been issued, to do this please use: M. N. PEERZADA, P. Khan, N. S. Khan, A. Gaur, F. Avecilla, Md. I. Hassan and A. Azam, *New J. Chem.*, 2020, DOI: 10.1039/D0NJ03474F.

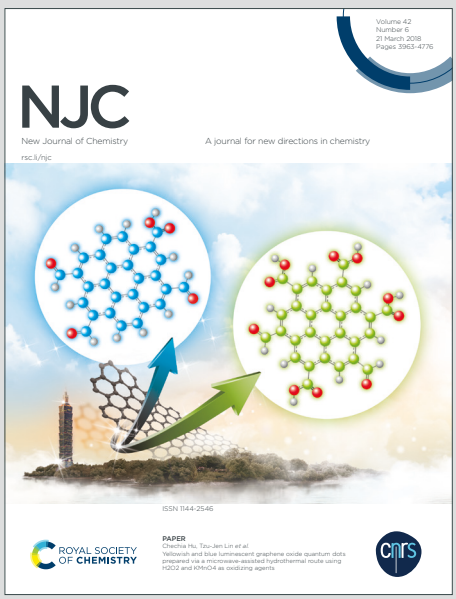

View Article Online
DOI: 10.1039/D0NJ03474F

Identification of morpholine based hydroxylamine analogues: Selective inhibitors of MARK4/Par-1d causing cancer cell death through apoptosis

Mudasir Nabi Peerzada[1], Parvez Khan[2], Nashrah Sharif Khan[2,3], Aysha Gaur[1], Fernando Avecilla[4], Md. Imtaiyaz Hassan[2], Amir Azam[1,*]

[1]*Medicinal Chemistry Research Laboratory, Department of Chemistry, Jamia Millia Islamia, Jamia Nagar, New Delhi-110025, India.*

[2]*Centre for Interdisciplinary Research in Basic Sciences, Jamia Millia Islamia, Jamia Nagar, New Delhi-110025, India.*

[3]*Department of Biotechnology, Jamia Millia Islamia, Jamia Nagar, New Delhi-110025, India.*

[4]*Grupo Xenomar, Centro de Investigacións Científicas Avanzadas (CICA), Departamento de Química, Facultade de Ciencias, Universidade da Coruña, Campus A Coruña, 15071, A Coruña, Spain.*

---

* *Corresponding author:* E-mail address: amir_sumbul@yahoo.co.in (A. Azam).
Tel.: +91-11-26981717/3254; fax: +91 11 26980229

View Article Online
DOI: 10.1039/D0NJ03474F

Abstract

Microtubule affinity-regulating kinase 4 (MARK4) is a serine/threonine kinase involved in the phosphorylation of MAP proteins that regulate microtubule dynamics and abets tumor progression by participating in oncogenic signaling pathways. It is overexpressed in multiple human malignancies and no drug is available for this potential therapeutic target at present. Therefore, using the structure based drug design strategy, a library of hydroxylamine derivatives of morpholine were designed and synthesized as small molecule inhibitors of MARK4. Compound **32** having CF_3 group at the *ortho* position of phenyl ring tethered with >C=NOH core and the hinge binder morpholine component, was found as potent and selective inhibitor of MARK4 over other thirty serine-threonine kinases. Study of cell viability and compound induced morphological changes in MCF-7 cancer cells discovered that molecule **32** caused death of cancerous cells through mechanism of apoptosis. Compound **32** may be transported and delivered to the target site through blood stream, and has promising antioxidant potential. Such bio-active molecules could serve as optimized lead candidates in drug discovery for cancer treatment through MARK4 inhibition.

Keywords: Hydroxylamine, Morpholine, Small-molecule inhibitors, Crystal structures, MARK4 inhibitors, Apoptosis

View Article Online
DOI: 10.1039/D0NJ03474F

1. Introduction

Microtubule Affinity-Regulatory Kinase 4 (MARK4), also termed as Par-1d, is a member of Ser/Thr kinase family that has surfaced as an important therapeutic target for drug development against cancer. It belongs to the calcium/calmodulin-dependent protein kinases and is involved in catalyzing the transfer of the γ-phosphate group of ATP to the microtubule-associated proteins (MAPs).[1] The process of phosphorylation maintains the cell polarity, microtubules stability, protein stability, intracellular signaling, cell cycle control, cell division specifically in the G1/S checkpoint and many other complex cellular processes due the detachment of MAPs from microtubule assembly.[2,3] Phosphorylation by MARK4 at Thr214 residue activates the microtubule dynamics and at Ser218 residue of Lys-Xaa-Gly-Ser (KXGS) motifs inhibits its function. The active site residue Asp181 gets activated through the phosphorylation of Thr214.[4,5]

MARK4 gets expressed almost in every organ of human body and its up-regulation facilities the development of glial tumors, lung carcinoma and leukemia.[5] MARK4 plays a significant role in Wnt signaling pathway and is associated with β-catenin/TCF-dependent transcription activity that leads to prostate cancer development.[6] The overexpression of MARK4 is also allied with nuclear accumulation of β-catenin in hepatic cells that promotes hepatocellular carcinogenesis.[7] Recent reports have established its involvement in breast cancer progression, migration and metastasis development. MARK4 up-regulation in breast cancer cells excels the proliferation by inhibiting Hippo signaling pathway.[8] The obstruction of phosphorylation process carried out by MARK4 seems to be one of the promising chemotherapeutic management strategies of breast cancer.[9] The conclusive findings related to the up-regulation of MARK4 in multiple human malignancies, interference with signal transductions and its occurrence as a negative regulator of mTORC1[6], marks it as a potent target for cancer treatment.

View Article Online
DOI: 10.1039/D0NJ03474F

Mostly the kinase inhibiting agents are reversible, ATP-competitive and bind in the ATP-binding pocket. It has been documented that morpholine based drugs pictilisib (GDC-0941) (**1**) and gilteritinib (**2**) are the FDA approved kinase inhibitors that function by interacting with the ATP-binding domain of kinases (**Figure 1**).[10,11] Some morpholine derivatives that have been reported as selective ATP-competitive inhibitors are proposed to act as the hinge-region binders in PI3K/mTOR inhibitors.[12,13] Moreover, the morpholine scaffold is introduced in the compounds of therapeutic potential for conferring the aqua solubility to the compounds and increasing the bioavailability.[12,14] Several Ser/Thr kinase inhibitors such as LY 294002 (**3**)[15], copanlisib (**4**)[16], buparlisib (**5**)[17] and GSK-263671 (**6**)[18] containing the morpholine scaffold have been described in literature.

Perusal of literature divulged that hydroxylamines act as key structural motif in several chemotypes endowed with anticancer activities including kinase inhibition.[19–22] Such compounds have been found to inhibit the kinase function by interacting at the ATP binding pocket and thereby prevent the phosphorylation process which in turn disrupts the microtubule assembly.[24] Designing hybrid molecules in which two or more pharmacophores are covalently linked is a rationally attractive approach toward the development of effective therapeutic molecules that have different modes of action and reduced side effects.[25] Further, the small molecule inhibitors play the pivotal role in the inhibition of various kinases pertaining to the human kinome and are being utilized extensively in the drug development. The small molecule ATP competitors have the major access to interact with the active cleft residues of the kinases and hence show maximum inhibition potential.[26,27]

In addition, as the MARK4 expression plays crucial role in the induction of oxidative stress in adipocytes and therefore, the inhibition of MARK4 may result into the reduction of

View Article Online
DOI: 10.1039/D0NJ03474F

reactive oxygen species (ROS) generation which thereby relieves the oxidative stress in cells and prevents oncogenesis.[28,29] The hydroxylamines are reported to be the potent radical scavengers and hence possess the significant antioxidant potential.[30,31] Considering the important pharmacological properties such as ease in diffusion, membrane permeability, transport, bioavailability, binding affinity, potency associated with small ring heterocyclic motifs[32–36] and our earlier reports on microtubule affinity-regulating kinase 4[37–39], we herein report the design and synthesis of novel hydroxylamine derivatives of morpholine as a new class of potent MARK4 inhibitors with substantial antioxidant potential.

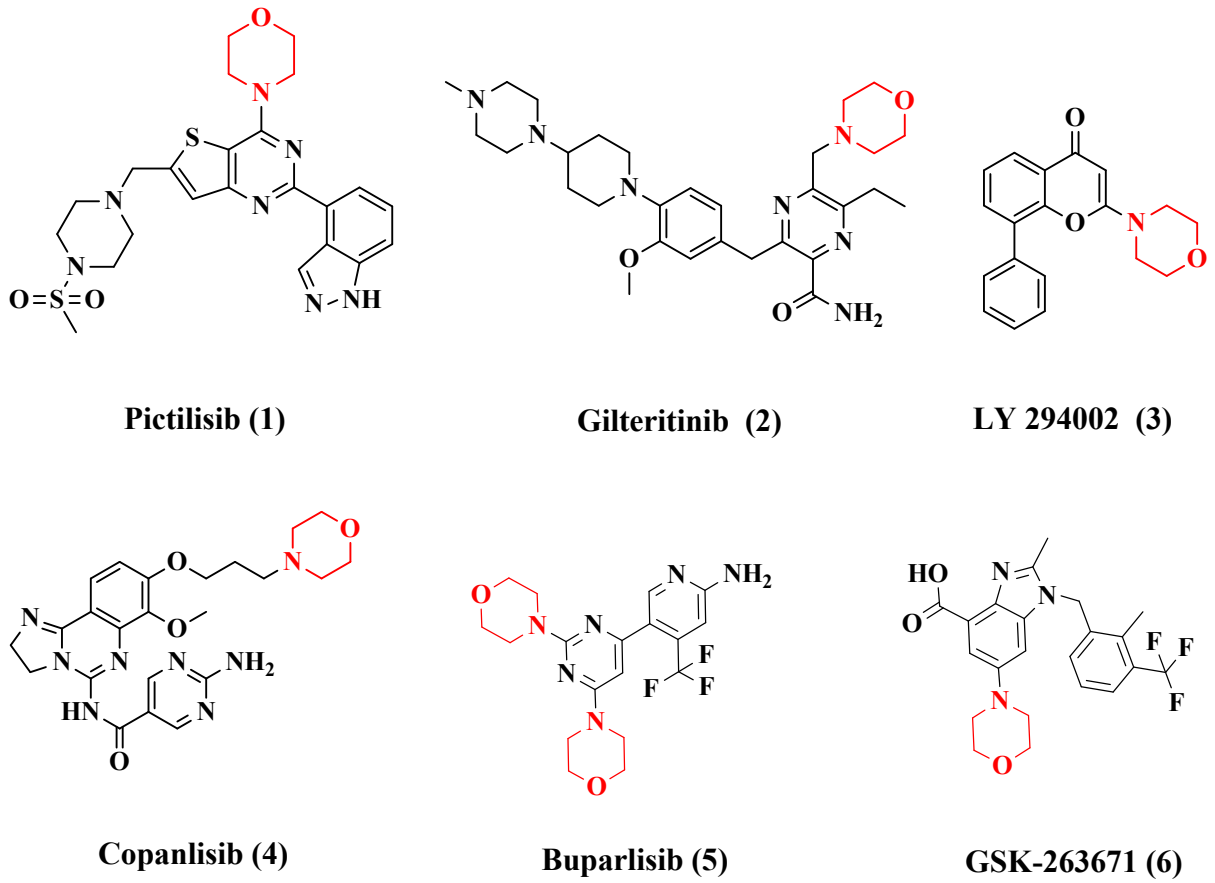

Figure 1. Morpholine heterocyclic scaffold in some potent Ser/Thr kinase inhibitors.

View Article Online
DOI: 10.1039/D0NJ03474F

2. Results and Discussion

2.1. Chemistry

In the context of our ongoing endeavor for MARK4 inhibitor development, a series of morpholin-4-yl-methylidene hydroxylamines (**Scheme 1**) were synthesized from substituted aldehydes (**1-8**) which were converted into their corresponding arylaldoximes (**9-16**) in presence of hydroxylamine hydrochloride under low temperature. The arylaldoximes (**9-16**) were then chlorinated in presence of *N*-Chlorosuccinimide (NCS) and dimethylformamide (DMF) to get carboximidoyl chlorides (**17-24**). These intermediates were reacted with morpholine in presence of hindered base triethylamine (TEA) to form arylhydroxylamine derivatives of morpholine (**25-32**). All the synthesized compounds were characterized by using various analytical techniques such as ^{1}H NMR, ^{13}C NMR, ESI-MS and their purity was established by elemental analysis (CHNS). All compounds have a purity grade of ≥ 95%.

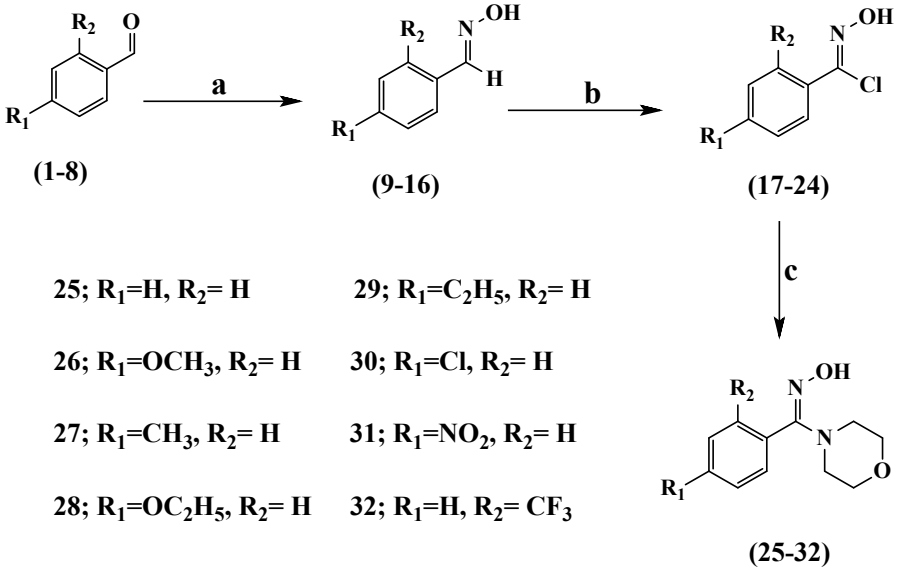

Scheme 1. *Reagents and conditions: (a) $NH_4OH.HCl$, 3N NaOH, EtOH, reflux, 14-20 h; (b) NCS, DMF 60 ˚C 8-12 h; (c) morpholine, DCM, TEA, 0 ˚C, 15-20 h.*

View Article Online
DOI: 10.1039/D0NJ03474F

2.2. X-ray Crystallography

Crystals suitable for measuring by X-ray crystallography were found for the compounds **25, 28** and **32**. Compound **25** crystallizes in orthorhombic crystal system and compounds **28** and **32** in triclinic crystal system (**Table 1**). The compound **25** contains two molecules in the asymmetric unit, which correspond with two atropoisomers (**Figure S1**). These atropoisomers are present in all the structures. In **25**, a large Flack parameter, 0.6(14), was observed and Friedel pairs were determined and their number was 25280. **Figure 2** shows a drawing of probability ellipsoids of the compounds **25**, **28** and **32**. Bond lengths and angles are similar to other morpholine derivatives with hydroxilamines (**Table S1**). Intermolecular hydrogen bonds appear in the structures and they are summarized in **Table S2**.

Non covalent interactions are important in the crystal packing (**Figure 3**). In compound **25**, the principal interaction is between non-binding pair of the oxygen atoms of hydroxylamine groups and -CH_2- groups of morpholine rings (~ 2.6 Å). In compound **28**, C-H$\cdots\pi$ (~ 2.8 Å) interactions, between -CH_2- groups and π clouds of the phenyl rings and interactions between the non-binding pair of the oxygen atoms of substituents with -CH_2- of morpholine groups (~ 2.6 Å) are the more intense. In compound **32**, fluorine atoms interact with hydrogen atoms of sp^3 carbons of morpholine rings of the next molecules (~ 2.6 Å) and the morpholine groups form an antiparallel sandwich structures by -CH_2- groups and non-binding pair of the oxygen atoms of morpholine groups interactions (~ 2.66 Å). Differences in the predominant interactions may explain the different behavior of these compounds when interacting with MARK4 target.

View Article Online
DOI: 10.1039/D0NJ03474F

Table 1. Crystal Data and Structure Refinement for the Compounds **25**, **28** and **32**

Compound	**25**	**28**	**32**
Formula	$C_{11}H_{14}N_2O_2$	$C_{13}H_{18}N_2O_3$	$C_{12}H_{13}F_3N_2O_2$
Formula weight	206.24	250.29	274.24
T, *K*	100(2)	100(2)	100(2)
Wavelength, Å	0.71073	0.71073	0.71073
Crystal system	Orthorhombic	Triclinic	Triclinic
Space group	$Pna2_1$	$P\bar{1}$	$P\bar{1}$
a/Å	19.6320(10)	6.8280(3)	7.2135(9)
b/Å	5.7579(3)	8.4251(4)	9.5319(10)
c/Å	18.7135(11)	12.0384(5)	9.6366(11)
α/°	90	101.2290(10)	84.670(4)
β/°	90	95.1410(10)	68.742(4)
γ/°	90	109.126(2)	82.721(4)
V/Å^3	2115.4(2)	632.92(5)	611.74(12)
Z	8	2	2
F_{000}	880	268	284
D_{calc}/g cm^{-3}	1.295	1.313	1.489
μ/mm^{-1}	0.091	0.094	0.132
θ/ (°)	3.01 to 28.31	2.63 to 28.32	3.05 to 28.34
R_{int}	0.1073	0.0579	0.0482
Crystal size/ mm^3	0.08 x 0.20 x 0.22	0.11 x 0.11 x 0.18	0.05 x 0.17 x 0.20
Goodness-of-fit on F^2	1.041	1.036	1.038
$R_1[I>2\sigma(I)]$ [a]	0.0472	0.0402	0.0435
wR_2 (all data) [b]	0.1079	0.1027	0.0976
Largest differences peak and hole (eÅ^{-3})	0.168 and -0.224	0.421 and -0.211	0.352 and -0.241

[a] $R_1 = \Sigma \left| |F_o| - |F_c| \right| / \Sigma |F_o|$. [b] $wR_2 = \{\Sigma[w(|F_o|^2 - |F_c|^2)^2]\} / \Sigma[w(F_o^2)^2]\}^{1/2}$

View Article Online
DOI: 10.1039/D0NJ03474F

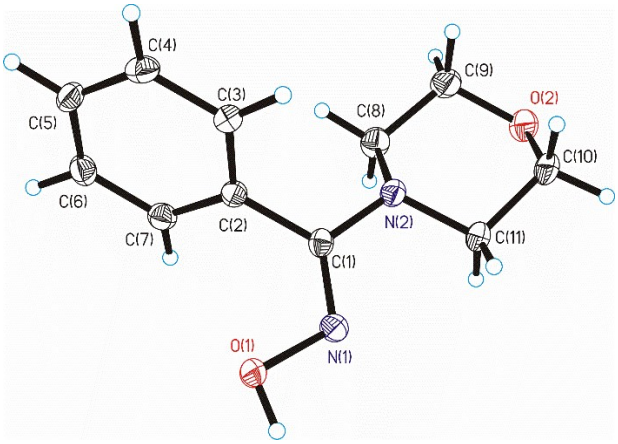

(25)

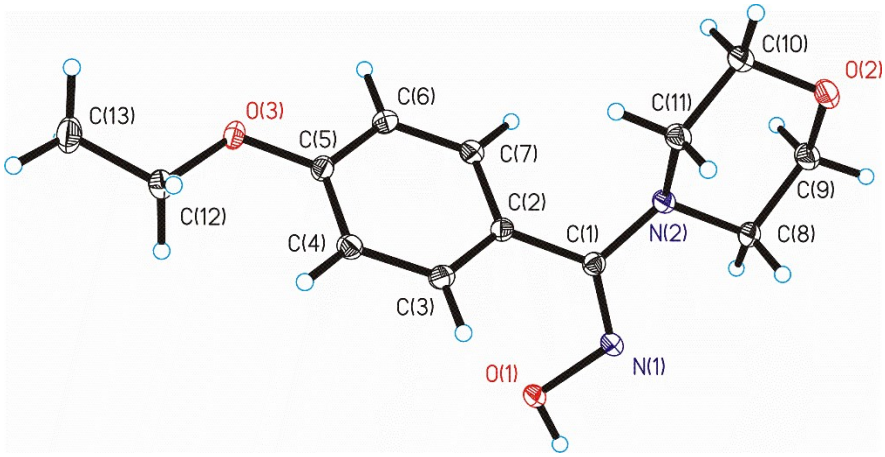

(28)

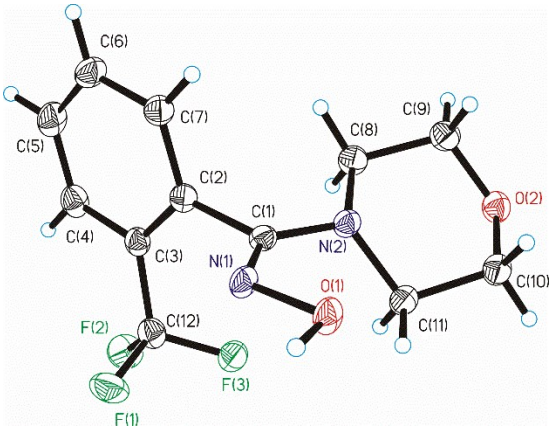

(32)

Figure 2. Molecular structures for morpholine derivatives **25**, **28** and **32**. All the non-hydrogen atoms are presented by their 50% probability ellipsoids. ORTEP drawing were done with SHELXL package.

View Article Online
DOI: 10.1039/D0NJ03474F

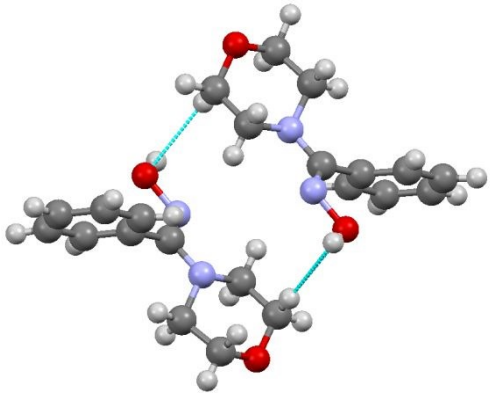

(25)

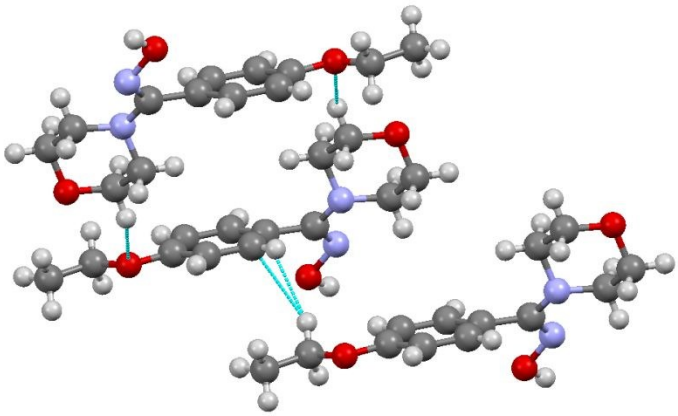

(28)

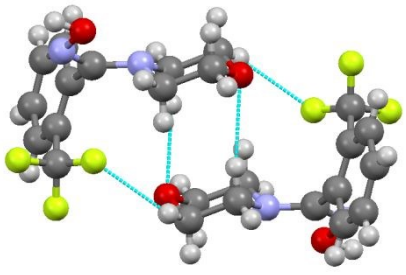

(32)

Figure 3. Non covalent interactions present in compounds **25**, **28** and **32**. Heteroatoms of different substituent's can determine the predominant interaction with the MARK4 target. Drawings were made with mercury 3.7 program in balls and sticks. Carbon

View Article Online
DOI: 10.1039/D0NJ03474F

atoms in gray, hydrogen atoms in white, nitrogen atoms in blue, oxygen atoms in red and fluorine atoms in yellow.

2.3. Molecular Docking

The binding mode of synthesized molecules (**25-32**) with amino acid residues of MARK4 was studied using molecular docking. Autodock Vina™ in combination with PyRx™ was employed to get a molecular insight of each MARK4-ligand complex.[40,41] Initially, the designed un-substituted molecule (**25**) of the series was subjected to docking for finding out the mode of interaction with MARK4. It was found that designed starting compound **25** showed efficient binding and interaction with the various active site residues of MARK4. The six membered morpholine ring of compound **25** showed π-alkyl interactions with Ala195 and Val70 whereas the hydrophobic phenyl substituent interacts with Ala83, Ala195, Val116, Met111, Val70 and Lys85 via π-alkyl interaction. The nitrogen atom of the -NOH group shows polar interaction with Asp196 whereas its hydrogen atom forms the hydrogen bond with Lys85 residue (**Figure S2**).

The binding energy and MARK4 residues interacting with each of the synthesized ligand is provided in supporting information **(Table S3**, **Figures S2-S5)**. All synthesized compounds showed significant binding energy in the range of –6.2 kcal/mol to –7.1 kcal/mol. It was found that the complex of MARK4 with synthesized ligands **25-32** was stabilized by substantial number of non-covalent interactions such as hydrogen bonding, van der Waals forces that are formed with the active site residues of MARK4 (**Figures S2-S5**). The consistency of docking protocol was examined by re-docking the known inhibitor of MARK4 (pyrazolopyrimidine inhibitor 5RC, **Figure S5D-E**) into the active site of the MARK4[52].

2.4. MARK4 Inhibition and Structure Activity Relationship (SAR)

View Article Online
DOI: 10.1039/D0NJ03474F

After the *in silico* evaluation of binding affinities of these compounds **25-32**, MARK4 enzyme inhibition studies was performed using ATPase assay. For conducting this study, we have expressed and purified recombinant MARK4 as described earlier.[42] For initial screenings, we performed single dose (20 μM) enzyme inhibition studies and found that compound **32** showed maximum inhibition potential at this dose. These studies suggested compound **32** as most active molecule, thus it was further evaluated for enzyme inhibition studies in the concentrations range of 0-20 μM (**Figure 4**). The cumulative results of docking and enzyme inhibition studies showed that compound **32** bind to the amino acid residues of MARK4 active site and inhibited its activity significantly (**Table 2**).

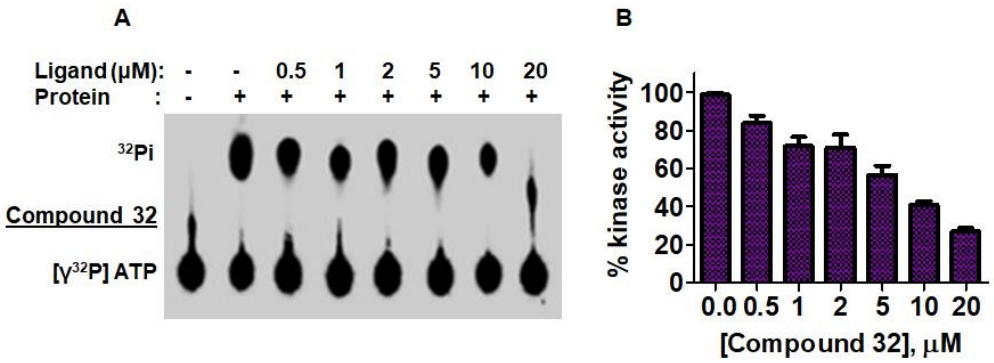

Figure 4. Enzyme inhibition studies of MARK4 with compound 32: (A) Shows the hydrolysis of ^{32}Pi from [γ-^{32}P] ATP, position of ^{32}Pi and ATP spots are indicated. Lane 1, negative control (no protein); lane 2, 100 nM MARK4 (positive control); and lanes labeled as 0.5, 1, 2, 5, 10 and 20 shows the concentration of compound **32**; **(B)** ATPase inhibition (% hydrolysis of Pi) with increasing concentrations of compound **32** is shown as a function of concentration quantified by comparing with positive control.

The scaffold variation was performed on the either side of the >C=NOH core for finding out the impact of the varied electronic arrangement on the MARK4 enzymatic activity by the target molecules **25-32**. All the evaluated compounds of the **Scheme 1** share the common structural features of central >C=NOH core and hydrophobic substituent. The hydroxylamine

View Article Online
DOI: 10.1039/D0NJ03474F

group was coupled with morpholine ring which acts as the hinge region binder in most of the kinase inhibitors. The initial compound **25** bearing unsubstituted phenyl ring was observed to be less potent when evaluated for MARK4 inhibitory activity. However, the introduction of electron releasing groups (ERGs) such as OCH_3 (**26**), CH_3 (**27**), C_2H_5 (**28**) and Cl (**30**) at C-4 position in phenyl ring as R_1 substituents still lead to the minimal MARK4 inhibition except that of OC_2H_5 (**29**) which resulted in improved enzymatic activity (**Figure 5)**. The replacement of these ERGs with strongly electron withdrawing NO_2 group (**31**) at the same position resulted into the slight enhancement in the potency. Surprisingly, multifold MARK4 inhibition was noticed when CF_3 group was incorporated as R_2 substituent in the phenyl ring and keeping the R_1 as H atom (**Table 2**).

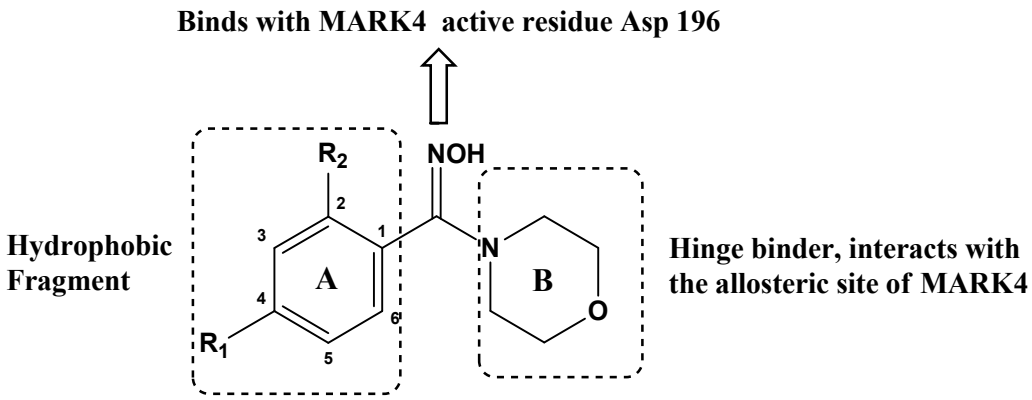

Figure 5. Structure of the designed molecules depicting the tactical variation on either side of hydroxylamine central core.

Since the MARK4 inhibitory activity shown by the electron withdrawing groups was more effective as compared to the ERGs in **Scheme 1**. Therefore, in terms of structure activity relationship, it can be concluded that the MARK4 inhibition of studied molecules was substituent dependent. The compound **32** that has –CF3 group was most potent among all other chemotypes which supported the earlier reports that the molecules bearing trifluoromethyl group occupy prime importance in the medicinal chemistry due to their significant drug like properties such as

View Article Online
DOI: 10.1039/D0NJ03474F

momentous lipophilicity, absorption and metabolic stability.[43,44] Moreover, the presence of –CF3 group may have drifted the activity of compound **32** due to its promising physiological significance mostly in terms of conferring the excellent lipophilicity and absorption to the molecule across the cellular plasma membrane for enhanced interaction with the MARK4 enzyme.

Table 2. MARK4 and human cancer cell line proliferation inhibition profile of compounds **25-32**

Compound	R_1	R_2	MARK4 Inhibition IC_{50} (μM)	MCF-7 IC_{50} (μM)	HepG2 IC_{50} (μM)
25	H	H	>20	35.24	32.32
26	OCH_3	H	>20	30.43	29.44
27	CH_3	H	>20	27.52	26.33
28	OC_2H_5	H	14.34	22.34	20.77
29	C_2H_5	H	>20	33.24	30.22
30	Cl	H	>20	38.24	34.72
31	NO_2	H	19.54	24.41	28.27
32	H	CF_3	3.17	5.27	9.31
paclitaxel	-	-	-	0.05	0.07

2.5. Kinase Selectivity Profiling of Compound 32

Kinase inhibitors usually show off-target activities with same/different kinase families which are responsible for undesired side effects. Therefore, in order to check out the selectivity, the identified potent MARK4 inhibitor compound **32** was evaluated against a panel of 30 kinases of the same family (CAMK family). The results of kinase selectivity profiling showed that compound **32** inhibited the MARK4 more strappingly (>80%) as compared to other kinases of same family (**Figure 6**). It was found that, at the studied dose, out of 30 kinases, 23 kinases showed <20% inhibition, 6 kinases showed 20-40% inhibition and MARK4 showed >80%,

View Article Online
DOI: 10.1039/D0NJ03474F

indicating the remarkable selectivity of compound **32** towards MARK4 inhibition. The inhibition pattern indicated that at tested concentration, compound **32** moderately inhibited MARK1, CAMKIV and MAPKAPK2 and DAPK1 (**Table S4**). The reason behind these observations could be the similar architecture of binding pockets of these kinases. Taken together, the results of kinase selectivity clearly suggested that compound **32** showed high selectivity towards MARK4 inhibition.

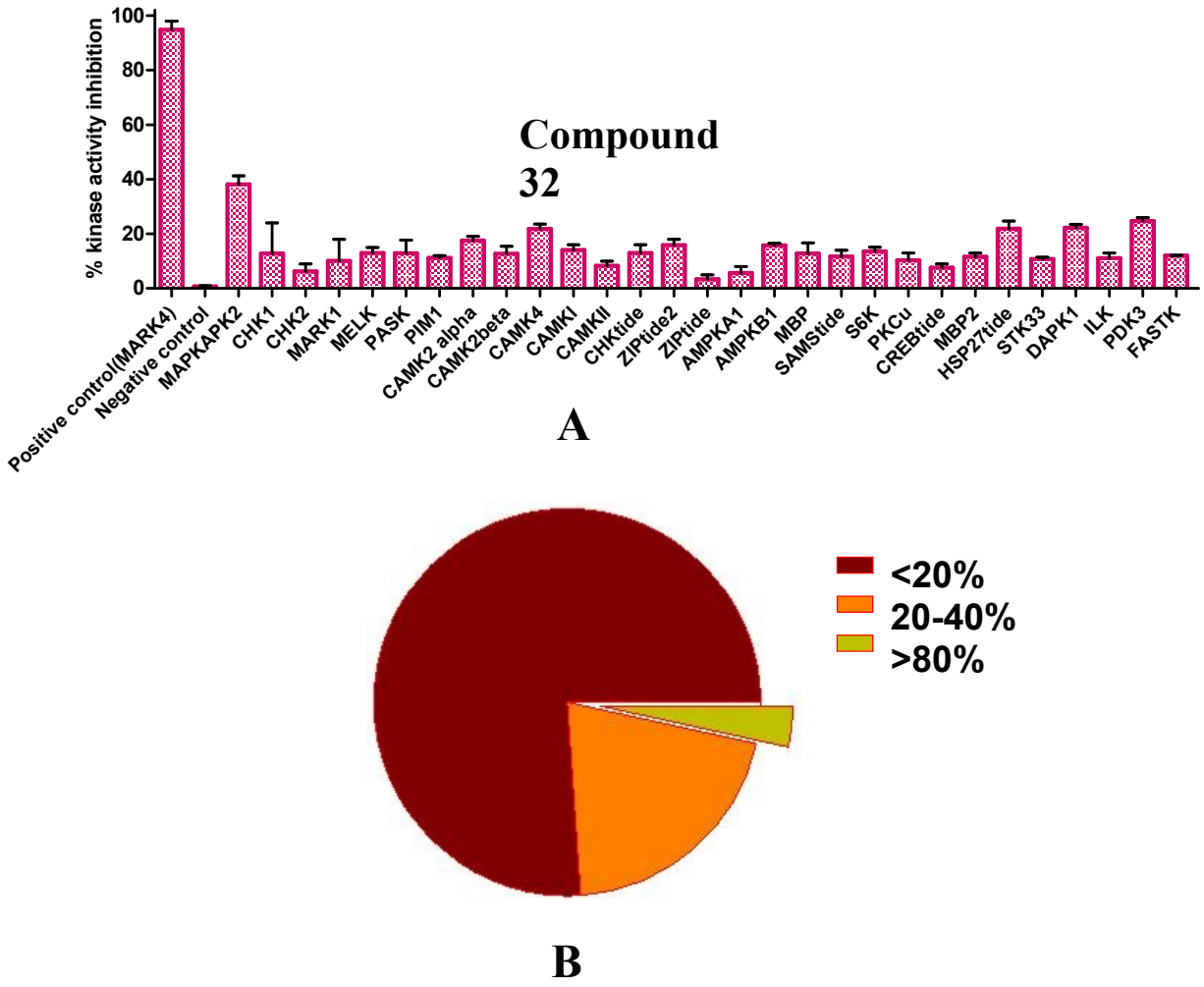

Figure 6. Single dose kinase selectivity assay: (A) Kinase inhibition results with a panel of 30 kinases for compound **32, (B)** Pie chart presentation for selectivity data. The selected panel of 30 kinases was incubated with 10µM dose of each compound and analyzed for percent activity values. The percent kinase activity was calculated and presented as a

View Article Online
DOI: 10.1039/D0NJ03474F

percentage of inhibition (%). In a total of 30 kinases, 23 kinases showed <20% inhibition, 6 kinases showed 20-40% inhibition and only MARK4 exhibit >80% inhibition.

2.6. Binding Affinity towards MARK4 and HSA

Binding studies of compound **32** with MARK4 and human serum albumin (HSA) was performed using fluorescence quenching method. Recombinant MARK4 was titrated with increasing concentrations of compound **32** and fluorescence emission was recorded. Similar experiment was carried out with HSA. The decrease in the fluorescence emission of MARK4/HSA was analyzed using modified Stern-Volmer relation (for details see Supporting Information) and binding constant K_a was estimated (**Figure 7**). The results showed that compound **32** possess high bonding affinity towards MARK4 with K_a value of 3.8×10^6 M^{-1}. However, for HSA the observed value of binding constant for compound **32** was 1.13×10^3 M^{-1}. These results advocated that compound **32** bind strongly with MARK4. The observed moderate binding affinity for the HSA indicates a desirable transport affinity and drug likeness of the molecule. HSA is the major carrier protein responsible for the transport of different molecules across the blood stream and thus the molecules as like compound **32** showing moderate affinities for HSA will be easy to transport.[37]

View Article Online
DOI: 10.1039/D0NJ03474F

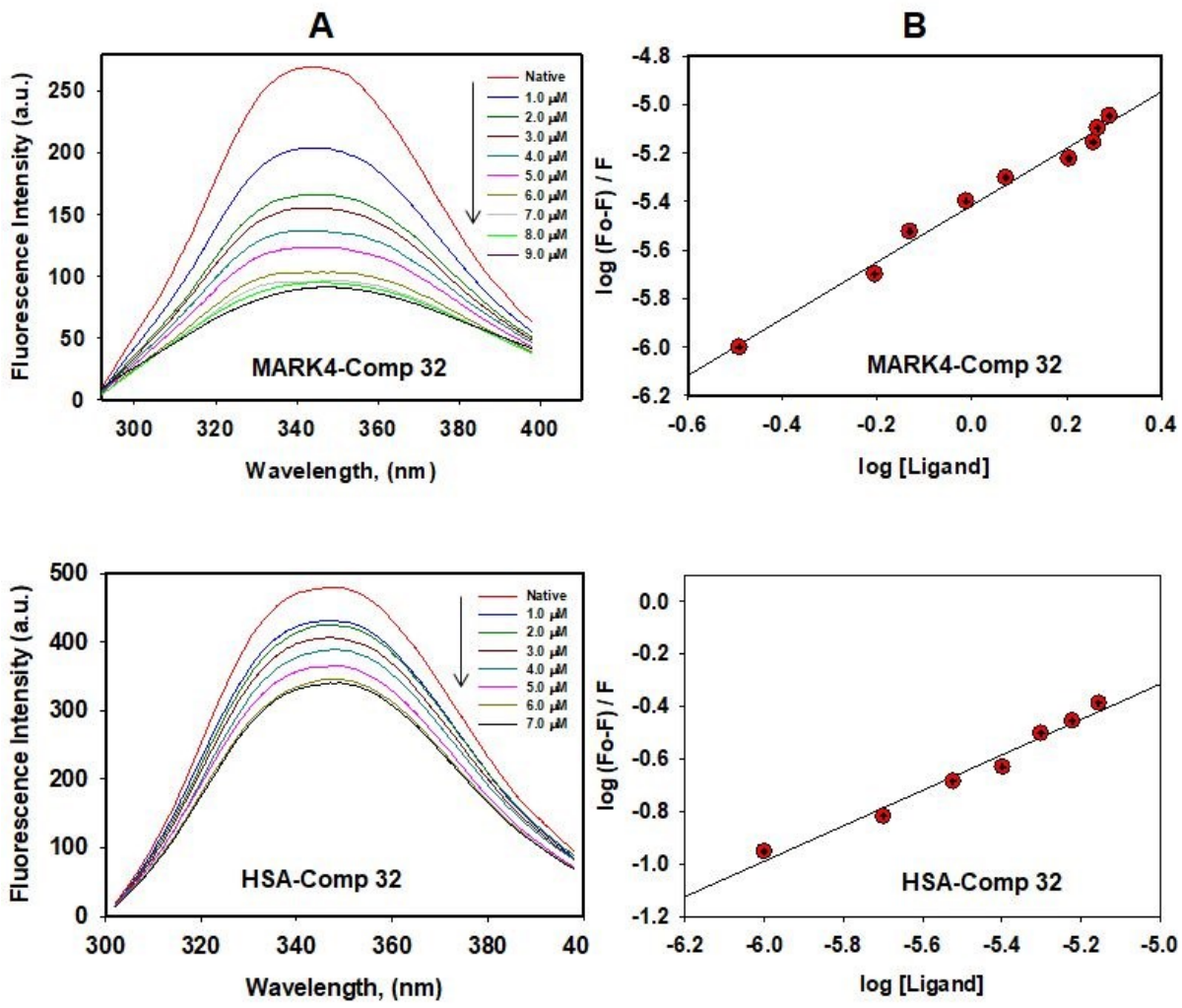

Figure 7. Fluorescence binding studies of compound 32 with MARK4 and HSA: (A) Fluorescence emission of MARK4 (10 μM)/HSA (25 μM) was recorded with the increasing concentrations of **32**. Emission spectrum showing quenching of MARK4/HSA fluorescence with the increasing concentration of compound **32** (excitation is at λ_{280} nm and emission range is 300-400 nm). **(B)** Showing the fitted fluorescence quenching data using Modified Stern-Volmer relation obtained from MARK4/HSA fluorescence with increasing concentration of **32.** This plot is used for the estimation of binding affinity (K_a).

2.7. Inhibition of Cancer Cell Proliferation

For the determination of antiproliferative potential of synthesized compounds **25-32** on human malignant cell lines MCF-7 and HepG2, MTT-based cell viability assay was performed. It was

View Article Online
DOI: 10.1039/D0NJ03474F

observed that compound **32** decreases the viability of MCF-7 and HepG2 cells in a dose dependent manner (**Figure 8A**). Interestingly, the toxicity evaluation of compound **32** on non-cancerous HEK293 cells showed that it did not affect the viability of these cells in the studied concentration range (**Figure 8B**). These observations suggested that compound **32** selectively inhibited the growth of MCF-7 and HepG2 cells as compared to HEK293 cells.

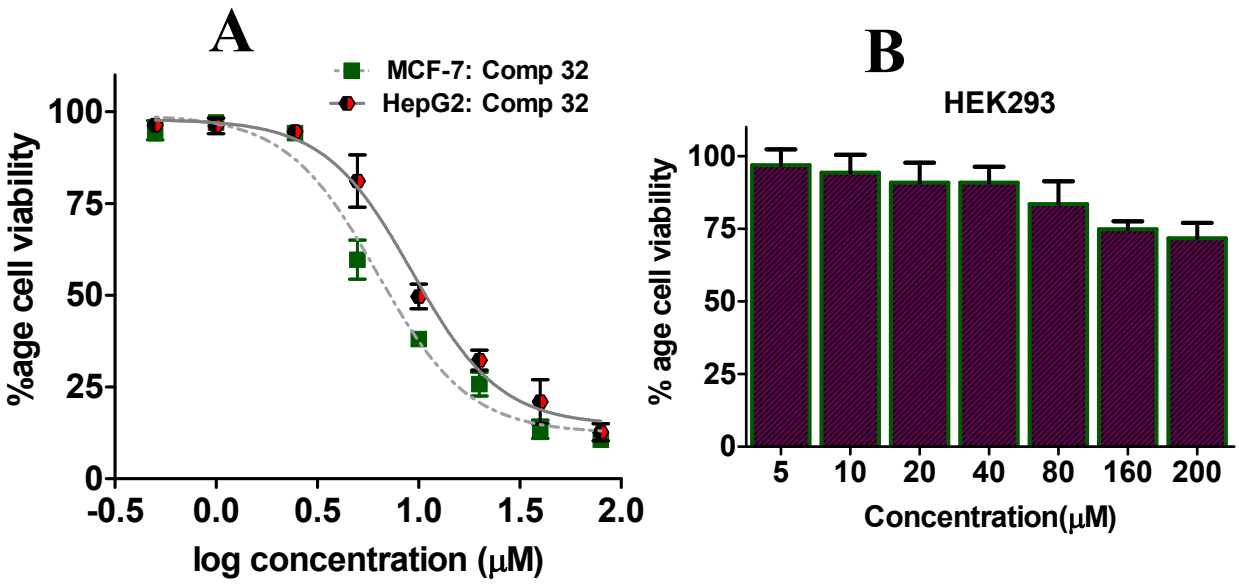

Figure 8. Cell viability studies: (A) Represents the effect of compound **32** on the viability of MCF-7 and HepG2 vs log concentration of compound **32**. **(B)** Graphical representation for cell viabilities of HEK293 cells. Each of selected cells was treated with increasing concentrations of compound **32** for 48 h. Cell viabilities were presented as the percentage of the number of viable cells to that of the control. Each data point shown is the mean ± SD from n=3. (For anticancer activities paclitaxel has been taken as positive control).

2.8. Apoptosis Studies

The compound **32** was evaluated for its apoptotic potential to understand the mechanism of action before its therapeutic implications. The MCF-7 and HepG2 cells were incubated with IC_{50} dose of compound **32** and apoptosis induction was studied using Annexin-V and PI staining. It was found that the treatment of compound **32** significantly induces apoptosis in MCF-7 and

View Article Online
DOI: 10.1039/D0NJ03474F

HepG2 cells as compared to vehicle controls (**Figure 9A-B**). Analysis of apoptosis results showed that compound **32** induce apoptosis in 26% of MCF-7 and 20.8% of HepG2 cells as compared to control cells. The results of these studies suggested that, in MCF-7 and HepG2 cells compound **32** induces cell death through mechanism of apoptosis. Interestingly, present apoptosis studies are in concurrence with earlier reports which emphasized that the inhibitors or inhibition of MARK4 induces apoptosis in MCF-7, HepG2 and other cancerous cells.[38,45,46]

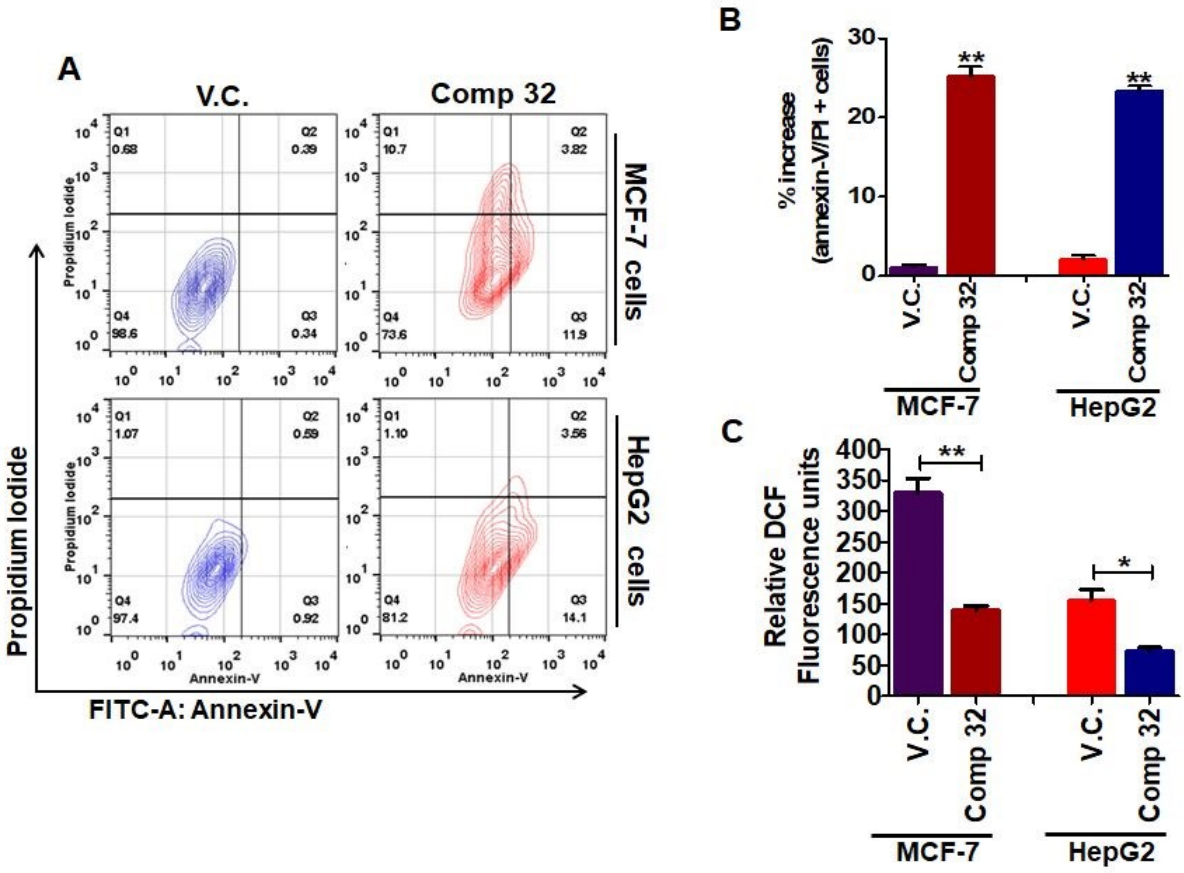

Figure 9. Compound 32 induces apoptosis and decreases the production of ROS. (A) Representative contour plots showing the anti-FITC-Annexin-V and PI stained cells after the treatment of compound **32**; name of cell line is indicated on right side of the plot. The MCF-7 and HepG2 cells were treated with IC_{50} concentrations of compound **32** for 48 h and processed for apoptosis analysis using Annexin-V/PI apoptosis kit. **(B)** Bar graphs represent the percentage of apoptotic cells stained with Annexin-V/PI for triplicate measurements ± SD. **(C)** Graphical representation for DCF fluorescence,

View Article Online
DOI: 10.1039/D0NJ03474F

MCF-7 and HepG2 cells were treated with compound **32** and analyzed for the ROS using H2DCFDA staining. Student t-test was used for statistical analysis, *p< 0.05, **p< 0.01, compared with the vehicle control.

2.9. Determination of Reactive Oxygen Species (ROS) Level

Cellular redox status plays an important role in regulation of different signaling pathways and growth maintenance. Respiration and metabolic pathways are the main sources of free radical production.[47] Contrary to normal cells, cancer cells creates their own redox environment that plays an important role in cancer cell growth and progression.[48] Hydroxylamines are known to decrease the production of reactive oxygen species (ROS), thus we were interested to investigate the radical scavenging capability of the compound **32**. It was observed that after the treatment of MCF-7 and HepG2 cells with compound **32**, the DCF fluorescence deceases, which suggested a decrease in the levels of cellular ROS (**Figure 9C**). It has also been reported previously that overexpression of MARK4 promotes the oxidative stress and therefore inhibition of MARK4 decreases the ROS levels.[29] The results of ROS studies are also in close agreement with earlier reports that inhibition of MARK4 decreases the ROS generation and thus controls cancer cell growth and proliferation. In the present study, we consider that the significant antioxidant potential of compound **32** in MCF-7 and HepG2 cells is most probably due the synergistic effect of free –NOH group, structural features of molecule and the MARK4 inhibition potential, as both hydroxylamines and MARK4 inhibition have been independently reported for causing the reduction of ROS in different cancer cells.[30,31,45]

In addition, all the compounds were observed of having appreciable water solubility in the range of 24±0.01to 85±1.1 mg/mL indicating their efficient bioavailability (**Table S5**). Often the FDA approved kinase inhibitors/drugs are difficult to synthesize and involve harsh chemical reactions. In compendium, the ease of synthesis, small molecule nature, least off target

View Article Online
DOI: 10.1039/D0NJ03474F

interactions and significant antioxidant potential associated with our synthesized molecules, adds them as a new class of compounds as potent MARK4 inhibitors. The molecular hybridization of the morpholine scaffold with the substituted hydroxylamine scaffold led to the emergence and identification of the novel potent MARK4 inhibitors, envisaged with appreciable bioavailability, anti-proliferative, and apoptotic activities

3. Conclusions

Novel water soluble hydroxylamine derivatives of morpholine were designed and synthesized that emerged as small-molecule potent inhibitors of tumor associated MARK4. The compound **32** inhibited the enzymatic activity of MARK4 specifically and showed moderate effect on thirty other kinases of Seine/theronine family demonstrating the least off target interactions. *In silico* and fluorescence studies validated the strong affinity of compound **32** toward MARK4 enzyme. Mechanistically, the compound **32** inhibited the growth of cancerous cells through induction of apoptosis as revealed by Annexin-V and PI staining. In addition, the identified compound **32** surfaced as a significant antioxidant agent as it reduced the ROS level in MCF-7 and HepG2 cells. The observed potency of the compound **32** indicates that the presence of trifluromethyl group owns the promising pharmacological significance for the designing of the potent MARK4 inhibitors. The ascertained effectiveness of the designed compounds signifies the valuable importance of morpholine incorporating hydroxylamine derived small molecules for selective inhibition of MARK4, having remarkable antioxidant potential and efficient bioavailability. Compound **32** may serve as lead candidate for the designing of new inhibitors having enhanced therapeutic potential for the future clinical development in anticancer drug discovery paradigm through MARK4 inhibition.

View Article Online
DOI: 10.1039/D0NJ03474F

4. Experimental Section

4.1. Materials and Methods

Chemicals required were purchased from Sigma Aldrich Chemical Company (USA) and Merck All the chemicals were used as supplied as they were of analytical grade. Aluminum sheets (Percolated, Silica gel 60 F_{254}) of Merck Germany were used for thin-layer chromatography (TLC) purposes. For visualizing the reaction mixture spots on TLC, the ultraviolet light of wavelength (λ) = 254 nm was used. Melting points of the compounds were taken by the help of Veego instrument having model specifications of REC-22038 A2 and are uncorrected. ^{1}H NMR of the target compounds were recorded on Bruker Spectrospin DPX 300 MHz or Jeol-500 MHz spectrophotometers. ^{13}C NMR was recorded on a Bruker Spectrospin DPX 75 MHz or Jeol-125 MHz spectrometers and in both the cases $CDCl_3$ or DMSO-d_6 was used as a solvent and trimethylsilane (TMS) was taken as the internal standard. Splitting patterns of the peaks are designated as follows; s, singlet; d, doublet; t: triplet: m, multiplet; Ar: aromatic and morph: morpholine. ESI-MS (AB-Sciex 2000, Applied Biosystem) was used for recording the mass of the compounds. Percentage of elements in the compounds was checked by using CHNS analyzer elementar. Three-dimensional X-ray data were collected on a Bruker Kappa Apex CCD diffractometer.

Synthesis of Compounds (9-16 and **17-24)**. The synthesis of intermediates (**9-16**) and carboximidoyl chlorides (**17-24**) is given in Supporting Information.

4.2. Procedure for the synthesis of hydroxylamine derivatives of morpholine (25-32)

TEA (0.75mmol) was added to the morpholine (0.75mmol) taken in DCM followed by the drop wise addition of synthesized carboximidoyl chlorides (**17-24**, 0.75mmol). The reaction mixture was stirred for 15-20 hours at 0 ˚C and the progress of reaction was monitored by employing thin

View Article Online
DOI: 10.1039/D0NJ03474F

layer chromatography (TLC) visualized under 254nm UV irradiation. After completion, the reaction mixture was extracted with DCM and water. The DCM layer was washed with brine, dried over Na_2SO_4, filtered and concentrated *in vacuo* under reduced pressure. All the crude products were purified by column chromatography from hexane/ethyl acetate (1:1) as eluent to furnish the title compounds (**25-32**).

***N*-[(morpholin-4-yl)(phenyl)methylidene]hydroxylamine (25).** Yield: 91%; white solid; m.p: 105 ˚C. ^{1}H NMR (300 MHz, DMSO-d_6): δ 9.46 (s, 1H, N-OH), 7.66-7.37 (m, 5H, Ar-H), 3.62 (t, 4H, *J*=9.0 Hz, morph-CH_2), 2.89 (t, 4H, *J*= 9.0 Hz, morph-CH_2). ^{13}C NMR (75 MHz, DMSO-d_6): 158.46, 131.45, 129.46, 129.28, 128.58, 66.27, 48.29. ESI-MS (m/z): [M + H] 207.23. Anal. Calcd. For $C_{11}H_{14}N_2O_2$: C, 64.06; H, 6.84; N, 13.58. Found: C, 64.13; H, 6.73; N, 13.57.

***N*-[(4-methoxyphenyl)(morpholin-4-yl)methylidene]hydroxylamine (26).** Yield: 89%; white solid; m.p: 107-108 ˚C. ^{1}H NMR (300 MHz, DMSO-d_6): δ 9.39 (s, 1H, N-OH), 7.45-7.29 (m, 2H, Ar-H), 6.99-6.91 (m, 2H, Ar-H), 3.79 (s, 3H, -OCH_3), 3.61 (m, 4H, morph-CH_2), 2.51-2.46 (m, 4H, morph-CH_2). ^{13}C NMR (75 MHz, DMSO-d_6): 159.97, 158.09, 131.06, 123.22, 113.94, 66.33, 55.58, 48.54. ESI-MS (m/z): [M + H] 237.20. Anal. Calcd. For $C_{12}H_{16}N_2O_3$: C, 61.00; H, 6.83; N, 11.86. Found: C, 61.13; H, 6.65; N, 11.87.

***N*-[(4-methylphenyl)(morpholin-4-yl)methylidene]hydroxylamine (27).** Yield: 91%; white solid; m.p: 105 ˚C. ^{1}H NMR (300 MHz, DMSO-d_6): δ 9.41 (s, 1H, N-OH), 7.42-7.17 (m, 4H, Ar-H), 3.61-3.44 (m, 4H, -CH_2 morph), 2.88-2.70 (m, 4H, morph-CH_2), 2.11 (s, 3H, -CH_3). ^{13}C NMR (75 MHz, DMSO-d_6): 158.41, 138.72, 129.44, 129.12, 128.42, 66.30, 48.38, 21.37. ESI-MS (m/z): [M + H] 221.04. Anal. Calcd. For $C_{12}H_{16}N_2O_2$: C, 65.43; H, 7.11; N, 12.72. Found: C, 65.51; H, 7.22; N, 12.79.

View Article Online
DOI: 10.1039/D0NJ03474F

***N*-[(4-ethoxyphenyl)(morpholin-4-yl)methylidene]hydroxylamine (28).** Yield: 89%; white solid; m.p: 108 ˚C. ^{1}H NMR (300 MHz, DMSO-d_6): δ 9.40 (s, 1H, N-OH), 7.35 (d, 2H, *J*=8.4 Hz, Ar-H), 6.97 (d, 2H, *J*=8.4 Hz, Ar-H), 4.08-4.01 (q, 2H, -OCH_2), 3.60-3.59 (m, 4H, morph-CH_2), 2.87-2.84 (m, 4H, morph-CH_2), 1.36 (t, 3H, *J*=13.8 Hz, -CH_3). ^{13}C NMR (75 MHz, DMSO-d_6): 159.25, 131.06, 130.27, 123.05, 114.50, 67.22, 66.33, 63.51, 49.28, 48.55. ESI-MS (m/z): [M + H] 251.07. Anal. Calcd. For $C_{13}H_{18}N_2O_3$: C, 62.38; H, 7.25; N, 11.19. Found: C, 62.21; H, 7.30; N, 11.08.

***N*-[(4-ethylphenyl)(morpholin-4-yl)methylidene]hydroxylamine (29).** Yield: 90%; white solid; m.p: 107 ˚C. ^{1}H NMR (300 MHz, DMSO-d_6): δ 9.38 (s, 1H, N-OH), 7.41-7.11 (m, 2H, Ar-H), 6.96-6.90 (m, 2H, Ar-H), 4.08-4.01 (m, 4H, morph-CH_2), 3.61-3.58 (m, 4H, morph-CH_2), 2.87-2.84 (m, 2H, -CH_2), 1.36 (t, 3H, *J*=13.8 Hz, -CH_3). ^{13}C NMR (75 MHz, DMSO-d_6): 156.39, 147.45, 137.58, 130.52, 123.41, 66.60, 65.66, 48.64, 47.67, 21.27, 15.29. ESI-MS (m/z): [M + H] 235.19. Anal. Calcd. For $C_{13}H_{18}N_2O_2$: C, 66.64; H, 7.74; N, 11.96. Found: C, 66.56; H, 7.82; N, 11.85.

***N*-[(4-chlorophenyl)(morpholin-4-yl)methylidene]hydroxylamine (30).** Yield: 80%; white solid; m.p: 106 ˚C; ^{1}H NMR (500 MHz, $CDCl_3$): δ 8.55 (s, 1H, N-OH), 7.45 (d, 2H, , *J*=8.9 Hz, Ar-H), 6.97 (d, 2H, , *J*=8.9 Hz, Ar-H), 3.68 (t, 4H, *J*=9.6 Hz, morph-CH_2), 2.99 (t, 4H, *J*=9.6 Hz, morph-CH_2). ^{13}C NMR (125 MHz, $CDCl_3$): 160.33, 159.64, 130.58, 122.00, 113.77, 55.20, 47.70. ESI-MS (m/z): [M + H] 101.25. Anal. Calcd. For $C_{11}H_{13}ClN_2O_2$: C, 54.89; H, 5.44; N, 11.64. Found: C, 54.97; H, 5.50; N, 11.53.

***N*-[(morpholin-4-yl)(4-nitrophenyl)methylidene]hydroxylamine (31).** Yield: 84%; yellow solid; m.p: 250 ˚C. ^{1}H NMR (500 MHz, $CDCl_3$): δ 9.26 (s, 1H, N-OH), 8.11 (d, 2H, , *J*=8.9 Hz,

View Article Online
DOI: 10.1039/D0NJ03474F

Ar-H), 7.66 (d, 2H, , *J*=8.9 Hz, Ar-H), 3.72 (t, 4H, *J*=9.6 Hz, morph-CH_2), 3.01 (t, 4H, *J*=9.6 Hz, morph-CH_2).^{13}C NMR (75 MHz, DMSO-d_6): 158.99, 148.34, 128.40, 110.48, 116.00, 66.60, 65.66, 48.64, 47.67. ESI-MS (m/z): [M + H] 252.12. Anal. Calcd. For $C_{11}H_{13}N_3O_4$: C, 52.59; H, 5.22; N, 16.73. Found: C, 52.71; H, 5.13; N, 16.84.

***N*-{(morpholin-4-yl)[2-(trifluoromethyl)phenyl]methylidene}hydroxylamine (32).** Yield: 91%; white solid; m.p: 258 ˚C. ^{1}H NMR (500 MHz, $CDCl_3$): δ 8.80 (s, 1H, N-OH), 7.69 (d, 1H, , *J*=7.5 Hz, Ar-H), 7.57-7.48 (m, 2H, Ar-H), 7.44 (d, 1H, , *J*=7.5 Hz, Ar-H), 3.65 (t, 4H, *J*=9.6 Hz, morph-CH_2), 3.29 (t, 4H, *J*=9.6 Hz, morph-CH_2). ^{13}C NMR (125 MHz, $CDCl_3$): 150.13, 111.25, 131.75, 129.96, 126.88, 126.67, 110.71, 122.52, 66.95, 66.29, 48.85, 46.54. ESI-MS (m/z): [M + H] 275.08. Anal. Calcd. For $C_{12}H_{13}F_3N_2O_2$: C, 52.56; H 4.78; N, 10.21. Found: C, 52.69; H, 4.85; N, 10.19.

4.3. X-Ray Crystal Structure Determination

Three-dimensional X-ray data were collected on a Bruker Kappa Apex CCD diffractometer at low temperature for compounds **25**, **28** and **32** by the ϕ-ω scan method. Reflections were measured from a hemisphere of data collected from frames, each of them covering 0.3º in ω. A total of 33309 for **25**, 26952 for **28** and 19936 for **32** reflections measured were corrected for Lorentz and polarization effects and for absorption by multi-scan methods based on symmetry-equivalent and repeated reflections. Of the total, 3860 for **25**, 2590 for **28** and 2320 for **32**, independent reflections exceeded the significance level ($|F|/\sigma|F|$) > 4.0 > 4.0. After data collection, in each case the multi-scan absorption correction (SADABS) [49] was applied, and the structure was solved by direct methods and refined by full matrix least-squares on F^2 data using SHELX suite of programs.[50] Hydrogen atoms were located in difference Fourier map and left to

View Article Online
DOI: 10.1039/D0NJ03474F

refine freely, except for C(13) in **28** which were included in calculation position and refined in the riding mode. Refinements were done with allowance for thermal anisotropy of all non-hydrogen atoms. A final difference Fourier map showed no residual density outside: 0.168 and -0.224 e.Å^{-3} for **25**, 0.421 and -0.211 e.Å^{-3} for **28** and 0.352 and -0.241 e.Å^{-3} for **32**. w = $1/[\sigma^2(F_o^2) + (0.045900\ P)^2 + 0.063900\ P]$ for **25**, $1/[\sigma^2(F_o^2) + (0.042100\ P)^2 + 0.293300\ P]$ for **28** and $1/[\sigma^2(F_o^2) + (0.030900\ P)^2 + 0.391100\ P]$ for **32**, where $P = (|F_o|^2 + 2|F_c|^2)/3$, were used in the latter stages of refinement. Further details of the crystal structures determination are given in **Table 1**. CCDC 1965979-1965981 numbers contain the supplementary crystallographic data for the structures reported in this paper. These data can be obtained free of charge via http://www.ccdc.cam.ac.uk/conts/ retrieving.html, or from the Cambridge Crystallographic Data Centre, 12 Union Road, Cambridge CB2 1EZ, UK; fax: (+44) 1223 336 033; or e-mail: deposit@ccdc.cam.ac.uk.

4.4. Molecular Docking

Molecular docking of the synthesized compounds **25-32** was carried out using Autodock Vina and AutoDock 4 package.[40,51] The structure coordinates of MARK4 was taken from Protein Data Bank (PDB ID 5ES1).[52] The 2D as well as 3D structures of all the synthesized hybrid molecules was drawn in ChemBio3D Ultra 12.0. Molecular docking was performed as described previously.[53] For visualization and structure analysis of the docked complexes of MARK4 and also to generate 2D docking for the analysis of hydrogen bonds and hydrophobic interactions, PyMOL viewer (Schrödinger, LLC) and "Receptor-Ligand Interactions" modules of BIOVIA/Discovery Studio 2017R2 were used.[54]

View Article Online
DOI: 10.1039/D0NJ03474F

4.5. Enzyme Inhibition Assay

To evaluate the enzymatic activity of MARK4, ATPase assay was performed in the presence of our synthesized molecules **25-32** as described earlier.[38,45] In brief, we have measured free ^{32}Pi generated from MARK4 arbitrated hydrolysis of [γ-^{32}P] ATP. Firstly, MARK4 was incubated alongwith ice-cold ATP (1 mM) having radioactive labeled [γ-^{32}P] ATP (specific activity 222 TBq mmol^{-1}) for 2 h at 37 °C and subsequently TLC studies was performed. The separated spots of hydrolyzed ^{32}Pi and ATP were visualized using autoradiography. The inference of MARK4 inhibition in terms of percentage hydrolysis of ATP was quantified using imageJ software (https://imagej.nih.gov/ij/index.html).

4.6. Single Dose Kinase Inhibition Profiling of Compound 32

In vitro biochemical profiling of compound **32** was evaluated with the twenty six members of CAMK family (CAMK-1 and CAMK-2) of kinases using kinase screening kit by following the manufacturer's protocols (Promega, Madison, USA) as described previously.[37,55] Briefly, 10µM of synthesized compound along with 2µl of kinase solution was added to the corresponding well of assay plate. Serially, 2µl of kinase solution was added to each wells of the plate. The reaction mixture was gently mixed, centrifuged, and plate was incubated at room temperature (25 °C) for 10 minutes. Following the incubation period, 2µl of working stocks of ATP/substrate was added carefully to respective well. Mix the assay plate, centrifuge and incubate at room temperature (25 °C) for 60 minutes. Consequently, 5µl of ADP-Glo™ reagent was added to all reaction wells of the assay plate. Plate was mixed for 2 minutes, and incubated further at room temperature for 40 minutes. As a final point, 10µl of Kinase Detection Reagent was added to each reaction well and incubate the plate at room temperature for 30 minutes. After the completion of reaction,

View Article Online
DOI: 10.1039/D0NJ03474F

luminescence was measured using an integration time of 0.5 seconds per well. Using net luminescence of the no-compound control (negative control) reactions to represent 100% kinase activity, the percent kinase activity was calculated in the compound-containing reactions and plotted in terms of percent kinase activity inhibition. Additionally, as our lab is working on different human kinases such as calcium–calmodulin dependent protein kinase IV (CAMKIV), Fas-Activated Serine/Threonine Kinase (FASTK), PDK3 and Integrin linked kinase (ILK), so we have also study the selectivity/inhibition potential of compound **32** by malachite green assay as per our previously reported protocol.[56]

4.7. Fluorescence Measurements

Binding affinities of compound **32** MARK4 and HSA was performed using the fluorescence spectroscopy as per our published protocol.[56] The titration of protein was done in triplicates and for analysis their average was taken. The decrease in the fluorescence intensity of MARK4/HSA protein with the increasing concentration of compound **32** was used to calculate the binding constant (K_a) and the number of binding sites (n) present on the protein molecule by using the modified Stern-Volmer equation.[57]

$$\log (F_o\text{-}F)/F = \log K_a + n\log[L] \qquad (1)$$

where, F_o = Fluorescence intensity of native protein, F = Fluorescence intensity of protein in the presence of ligand, K_a = Binding constant, n = number of binding sites, L = concentration of ligand. The binding constant (K_a) and number of binding sites (n) were obtained from the intercept and slope, respectively.

View Article Online
DOI: 10.1039/D0NJ03474F

4.8. Cell Viability Assay

For cell viability studies, standard MTT assay was carried out as describe earlier.[45,56] Briefly, the MCF-7, HepG2 and HEK293 cells were plated at a density of 6000-7000 cells/well of a 96-well culture plate. After 24 h, cells were incubated with different concentrations (0.1–80 μM) of compounds **25-32** for 48 h at 37 °C in a humidified CO_2 incubator. After 48 h, the mixture of media and compounds was removed and 20 μl of MTT solution (from 5mg/ml stock solution in PBS, pH 7.4) along with 100 μl of cell growth medium was added to each well of the plate. The plates were incubated for 4-5 h at 37 °C in the CO_2 incubator and after the removal of supernatant, formazan crystals were dissolved in 100 μl of DMSO. The plates were agitated to mix the reaction content and the absorbance (A) of purple dissolved formazan was measured at 570/590 nm using an ELISA reader (Bio-Rad). The absorption was converted into percentage cell viability and used to estimate the IC_{50} (50% inhibitory concentration) values for synthesized compound**s**. For cell proliferation and anticancer activities paclitaxel was used as positive control.

4.9. Apoptosis Assay

Induction of apoptosis was analyzed using Annexin-V/PI staining as described previously.[42,56] Briefly, 2.5x 10^5 cells/well of a six well culture plate were plated and after 24 h growth, cells were incubated with IC_{50} concentration of **32** for 48 h at 37 ºC. The control cells were treated with vehicle control (PBS). After 48 h treatment, the cells were trypsinized and collected. The collected cells were washed three times with PBS and incubated with FITC- Annexin-V/PI in binding buffer using FITC-Annexin-V kit as per the manufacturer's instructions (BD-

View Article Online
DOI: 10.1039/D0NJ03474F

Biosciences, USA). Around, 10,000 events were collected for each sample using flow cytometry (BD LSR II Flow Cytometry Analyzer) and analyzed by FlowJo.

4.10. Investigation of Reactive Oxygen Species (ROS) Level

2′,7′-Dichlorodihydrofluorescein diacetate (H2DCFDA) staining was used for measuring the reactive oxygen species (ROS) production as described previously.[45,56] Briefly, the MCF-7 and HepG2 cells were plated at a density of 2.5x 10^5 cells/per well of the six well plate and on next day, cells were respectively treated with IC_{50} dose of compound **32** for 5-6 h (H_2O_2 is used as positive control). Subsequently, cells were incubated with DCFDA (10 μM) for 30 min in dark at 37 °C in a humidified CO_2 incubator. After 30 min incubation, the cells were washed with ice-cold PBS and harvested by trypsinization and collected by centrifugation. ROS levels were assessed by measuring the fluorescence of vehicle treated/compound treated cells at at Jasco spectroflourimeter (FP-6200) using a 5 mm quartz cuvette. The excitation and emission filters were set at 485/500-550nm, respectively.

4.11. Solubility Assay

20 mg of each the target compound **25-32** was taken in polypropylene microcentrifuge tube (2 mL strength) and 100 μL of citrate-buffered solution (pH 3.3) was added and then incubated on Eppendorf Thermomixer (1000 rpm) at 25 °C. The compounds were centrifuged at 20 800*g* for the time period of 2 minutes after incubation and then subjected to filtration through a 0.22 μm polyvinylidene difluoride (PVDF) membrane. Aliquots of the obtained filtrates were diluted by solvents DMSO/ acetonitrile (ACN)/ trifluoroacetic acid in the ratio of 80:20:0.1 and then kept at 4 °C. Agilent 1100 HPLC equipped with Waters Symmetry IS C18 column, (3.5 μm, 2.1×20 mm) accompanied with wavelength detection of 254 nm was employed for further analysis.

View Article Online
DOI: 10.1039/D0NJ03474F

Water (0.1% trifluoroacetic acid) and ACN (0.1% trifluoroacetic acid) systems were used as mobile phases while analysis. The column was eluted with 10% ACN (0.1% trifluoroacetic acid) for 0.5 minutes at first and then with 10% to 55% ACN (0.1% trifluoroacetic acid) over 9.5 minutes and finally at the gradient of 70% ACN (0.1% trifluoroacetic acid) for 1 minute at the flow rate of 1 mL/min. Peaks obtained were calibrated with the known standards and then the solubility was assessed.

Statistical Analysis. Data were expressed as mean ± standard error from three independent experiments. The statistical analysis of each data was performed using the two-tailed Student t-test for unpaired samples and value of $P<0.05$ were considered as significant.

Acknowledgements

Mudasir Nabi Peerzada is thankful to the Council of Scientific and Industrial Research, New Delhi, India for CSIR-SRF fellowship (F. No. 09/466 (0220) 2K19 EMR-I). This work is supported by the financial assistance from the Science and Engineering Research Board, Government of India (Project No. EMR/2015/002372). Parvez Khan thanks to the Department of Biotechnology, Government of India for the fellowship (BT/PR12828/AAQ/1/622/2015). Nashrah Sharif Khan acknowledges SRF from ICMR (No: 45/9/2019-PHA/BMS). We sincerely acknowledge Harvard University-plasmid providing facility for providing the *MARK4* gene. We thank Almanac Life Sciences India Private Limited and Piquant Scientific Private Limited for helping us in kinase profiling studies.

Conflict of Interest

The authors declare no conflict of interest.

View Article Online
DOI: 10.1039/D0NJ03474F

References

(1) Tassan, J.-P.; Le Goff, X. *Biol. cell* **2004**, *96* (3), 193–199.

(2) Drewes, G.; Ebneth, A.; Preuss, U.; Mandelkow, E. M.; Mandelkow, E. *Cell* **1997**, *89* (2), 297–308.

(3) Matenia, D.; Mandelkow, E.-M. *Trends Biochem. Sci.* **2009**, *34* (7), 332–342.

(4) Timm, T.; Li, X.-Y.; Biernat, J.; Jiao, J.; Mandelkow, E.; Vandekerckhove, J.; Mandelkow, E.-M. *EMBO J.* **2003**, *22* (19), 5090–5101.

(5) Naz, F.; Anjum, F.; Islam, A.; Ahmad, F.; Hassan, M. I. *Cell Biochem. Biophys.* **2013**, *67* (2), 485–499.

(6) Jenardhanan, P.; Mannu, J.; Mathur, P. P. *Mol. BioSyst.* **2014**, *10* (7), 1845–1868.

(7) Shen, X.; Liu, X.; Wan, S.; Fan, X.; He, H.; Wei, R.; Pu, W.; Peng, Y.; Wang, C. *Front. Chem.* **2019**, *7*.

(8) Heidary Arash, E.; Shiban, A.; Song, S.; Attisano, L. *EMBO Rep.* **2017**, *18* (3), 420–436.

(9) Naz, F.; Khan, F. I.; Mohammad, T.; Khan, P.; Manzoor, S.; Hasan, G. M.; Lobb, K. A.; Luqman, S.; Islam, A.; Ahmad, F.; et al. *Int. J. Biol. Macromol.* **2018**, *107* (Pt B), 2580–2589.

(10) Schöffski, P.; Cresta, S.; Mayer, I. A.; Wildiers, H.; Damian, S.; Gendreau, S.; Rooney, I.; Morrissey, K. M.; Spoerke, J. M.; Ng, V. W.; et al. *Breast Cancer Res.* **2018**, *20* (1), 109.

(11) Zhao, J.; Song, Y.; Liu, D. *Biomark. Res.* **2019**, *7*, 19.

(12) Andrs, M.; Korabecny, J.; Jun, D.; Hodny, Z.; Bartek, J.; Kuca, K. *J. Med. Chem.* **2015**, *58* (1), 41–71.

(13) Allen, C. E.; Welford, A. J.; Matthews, T. P.; Caldwell, J. J.; Collins, I. *Med. Chem. Commun.* **2014**, *5* (2), 180–185.

(14) Ohui, K.; Afanasenko, E.; Bacher, F.; Ting, R. L. X.; Zafar, A.; Blanco-Cabra, N.; Torrents, E.; Dömötör, O.; May, N. V; Darvasiova, D.; et al. *J. Med. Chem.* **2019**, *62* (2), 512–530.

(15) Vlahos, C. J.; Matter, W. F.; Hui, K. Y.; Brown, R. F. *J. Biol. Chem.* **1994**, *269* (7), 5241–5248.

(16) Eltantawy, A.; Vallejos, X.; Sebea, E.; Evans, K. *Ann. Pharmacother.* **2019**, *53* (9), 954–

View Article Online
DOI: 10.1039/D0NJ03474F

958.

(17) Wen, P. Y.; Touat, M.; Alexander, B. M.; Mellinghoff, I. K.; Ramkissoon, S.; McCluskey, C. S.; Pelton, K.; Haidar, S.; Basu, S. S.; Gaffey, S. C.; et al. *J. Clin. Oncol.* **2019**, *37* (9), 741–750.

(18) Li, B.; Sun, A.; Jiang, W.; Thrasher, J. B.; Terranova, P. *Am. J. Clin. Exp. Urol.* **2014**, *2* (3), 188–198.

(19) Qin, H.-L.; Leng, J.; Zhang, C.-P.; Jantan, I.; Amjad, M. W.; Sher, M.; Naeem-Ul-Hassan, M.; Hussain, M. A.; Bukhari, S. N. A. *J. Med. Chem.* **2016**, *59* (7), 3549–3561.

(20) Liu, F.; Park, J.-E.; Qian, W.-J.; Lim, D.; Scharow, A.; Berg, T.; Yaffe, M. B.; Lee, K. S.; Burke, T. R. *ACS Chem. Biol.* **2012**, *7* (5), 805–810.

(21) Cao, J.; Gao, H.; Bemis, G.; Salituro, F.; Ledeboer, M.; Harrington, E.; Wilke, S.; Taslimi, P.; Pazhanisamy, S.; Xie, X.; et al. *Bioorg. Med. Chem. Lett.* **2009**, *19* (10), 2891–2895.

(22) Choi, S.-J.; Lee, J.-E.; Jeong, S.-Y.; Im, I.; Lee, S.-D.; Lee, E.-J.; Lee, S. K.; Kwon, S.-M.; Ahn, S.-G.; Yoon, J.-H.; et al. *J. Med. Chem.* **2010**, *53* (9), 3696–3706.

(23) Meijer, L.; Skaltsounis, A.-L.; Magiatis, P.; Polychronopoulos, P.; Knockaert, M.; Leost, M.; Ryan, X. P.; Vonica, C. A.; Brivanlou, A.; Dajani, R.; et al. *Chem. Biol.* **2003**, *10* (12), 1255–1266.

(24) Leclerc, S.; Garnier, M.; Hoessel, R.; Marko, D.; Bibb, J. A.; Snyder, G. L.; Greengard, P.; Biernat, J.; Wu, Y. Z.; Mandelkow, E. M.; et al. *J. Biol. Chem.* **2001**, *276* (1), 251–260.

(25) Viegas-Junior, C.; Danuello, A.; da Silva Bolzani, V.; Barreiro, E. J.; Fraga, C. A. M. *Curr. Med. Chem.* **2007**, *14* (17), 1829–1852.

(26) Pollard, J. R.; Mortimore, M. *J. Med. Chem.* **2009**, *52* (9), 2629–2651.

(27) Peifer, C.; Abadleh, M.; Bischof, J.; Hauser, D.; Schattel, V.; Hirner, H.; Knippschild, U.; Laufer, S. *J. Med. Chem.* **2009**, *52* (23), 7618–7630.

(28) Cross, C. E.; Halliwell, B.; Borish, E. T.; Pryor, W. A.; Ames, B. N.; Saul, R. L.; McCord, J. M.; Harman, D. *Ann. Intern. Med.* **1987**, *107* (4), 526–545.

(29) Liu, Z.; Gan, L.; Chen, Y.; Luo, D.; Zhang, Z.; Cao, W.; Zhou, Z.; Lin, X.; Sun, C. *Sci. Rep.* **2016**, *6*, 21382.

(30) Ozen, T.; Taş, M. *J. Enzyme Inhib. Med. Chem.* **2009**, *24* (5), 1141–1147.

(31) Bergström, M. A.; Luthman, K.; Karlberg, A.-T. *Chem. Res. Toxicol.* **2007**, *20* (6), 927–

View Article Online
DOI: 10.1039/D0NJ03474F

936.

(32) Comess, K. M.; McLoughlin, S. M.; Oyer, J. A.; Richardson, P. L.; Stöckmann, H.; Vasudevan, A.; Warder, S. E. *J. Med. Chem.* **2018**, *61* (19), 8504–8535.

(33) Hameed, A.; Al-Rashida, M.; Alharthy, R. D.; Uroos, M.; Mughal, E. U.; Ali, S. A.; Khan, K. M. *Expert Opin. Ther. Pat.* **2017**, *27* (10), 1089–1110.

(34) Groner, B.; Weber, A.; Mack, L. *Bioengineered 3* (6), 320–325.

(35) Lawson, A. D. G.; MacCoss, M.; Heer, J. P. *J. Med. Chem.* **2018**, *61* (10), 4283–4289.

(36) Lipinski, C. A. *J. Pharmacol. Toxicol. Methods 44* (1), 235–249.

(37) Aneja, B.; Khan, N. S.; Khan, P.; Queen, A.; Hussain, A.; Rehman, M. T.; Alajmi, M. F.; El-Seedi, H. R.; Ali, S.; Hassan, M. I.; et al. *Eur. J. Med. Chem.* **2019**, *163*, 840–852.

(38) Parveen, I.; Khan, P.; Ali, S.; Hassan, M. I.; Ahmed, N. *Eur. J. Med. Chem.* **2018**, *159*, 166–177.

(39) Khan, P.; Queen, A.; Mohammad, T.; Smita; Khan, N. S.; Hafeez, Z. Bin; Hassan, M. I.; Ali, S. *J. Nat. Prod.* **2019**, *82* (8), 2252–2261.

(40) Trott, O.; Olson, A. J. *J. Comput. Chem.* **2010**, *31* (2), 455–461.

(41) Dallakyan, S.; Olson, A. J. *Methods Mol. Biol.* **2015**, *1263*, 243–250.

(42) Peerzada, M. N.; Khan, P.; Ahmad, K.; Hassan, M. I.; Azam, A. *Eur. J. Med. Chem.* **2018**, *155*, 13–23.

(43) Zhu, J.-Y.; Cuellar, R. A.; Berndt, N.; Lee, H. E.; Olesen, S. H.; Martin, M. P.; Jensen, J. T.; Georg, G. I.; Schönbrunn, E. *J. Med. Chem.* **2017**, *60* (18), 7863–7875.

(44) Johnson, L. N.; Lewis, R. J. *Chem. Rev.* **2001**, *101* (8), 2209–2242.

(45) Khan, P.; Rahman, S.; Queen, A.; Manzoor, S.; Naz, F.; Hasan, G. M.; Luqman, S.; Kim, J.; Islam, A.; Ahmad, F.; et al. *Sci. Rep.* **2017**, *7* (1), 9470.

(46) Li, L.; Guan, K.-L. *J. Biol. Chem.* **2013**, *288* (1), 703–708.

(47) Circu, M. L.; Aw, T. Y. *Free Radic. Biol. Med.* **2010**, *48* (6), 749–762.

(48) Schumacker, P. T. *Cancer Cell* **2006**, *10* (3), 175–176.

(49) Sheldrick, G. M. SADABS, Version 2.10. University of Gottingen, G. 2003.

(50) Sheldrick, G. M. *Acta Crystallogr. Sect. C, Struct. Chem.* **2015**, *71* (Pt 1), 3–8.

(51) Morris, G. M.; Huey, R.; Lindstrom, W.; Sanner, M. F.; Belew, R. K.; Goodsell, D. S.; Olson, A. J. *J. Comput. Chem.* **2009**, *30* (16), 2785–2791.

(52) Sack, J. S.; Gao, M.; Kiefer, S. E.; Myers, J. E.; Newitt, J. A.; Wu, S.; Yan, C. *Acta*

View Article Online
DOI: 10.1039/D0NJ03474F

Crystallogr. Sect. F, Struct. Biol. Commun. **2016**, *72* (Pt 2), 129–134.

(53) Anwar, S.; Shamsi, A.; Shahbaaz, M.; Queen, A.; Khan, P.; Hasan, G. M.; Islam, A.; Alajmi, M. F.; Hussain, A.; Ahmad, F.; et al. *Sci. Rep.* **2020**, *10* (1), 10300.

(54) BIOVIA, D. S. *San Diego: Dassault Syste`mes.* **2013**.

(55) Voura, M.; Khan, P.; Thysiadis, S.; Katsamakas, S.; Queen, A.; Hasan, G. M.; Ali, S.; Sarli, V.; Hassan, M. I. *Sci. Rep.* **2019**, *9* (1), 1676.

(56) Khan, N. S.; Khan, P.; Ansari, M. F.; Srivastava, S.; Hasan, G. M.; Husain, M.; Hassan, M. I. *Mol. Pharm.* **2018**, *15* (9), 4173–4189.

(57) Boaz, H.; Rollefson, G. K. *J. Am. Chem. Soc.* **1950**, *72* (8), 3435–3443.

View Article Online
DOI: 10.1039/D0NJ03474F

Identification of morpholine based hydroxylamine analogues: Selective inhibitors of MARK4/Par-1d causing cancer cell death through apoptosis

Mudasir Nabi Peerzada[1], Parvez Khan[2], Nashrah Sharif Khan[2,3], Aysha Gaur[1], Fernando Avecilla[4], Md. Imtaiyaz Hassan[2], Amir Azam[1,*]

[1]*Medicinal Chemistry Research Laboratory, Department of Chemistry, Jamia Millia Islamia, Jamia Nagar, New Delhi-110025, India.*

[2]*Centre for Interdisciplinary Research in Basic Sciences, Jamia Millia Islamia, Jamia Nagar, New Delhi-110025, India.*

[3]*Department of Biotechnology, Jamia Millia Islamia, Jamia Nagar, New Delhi-110025, India.*

[4]*Grupo Xenomar, Centro de Investigacións Científicas Avanzadas (CICA), Departamento de Química, Facultade de Ciencias, Universidade da Coruña, Campus A Coruña, 15071, A Coruña, Spain.*

For Table of Contents Only

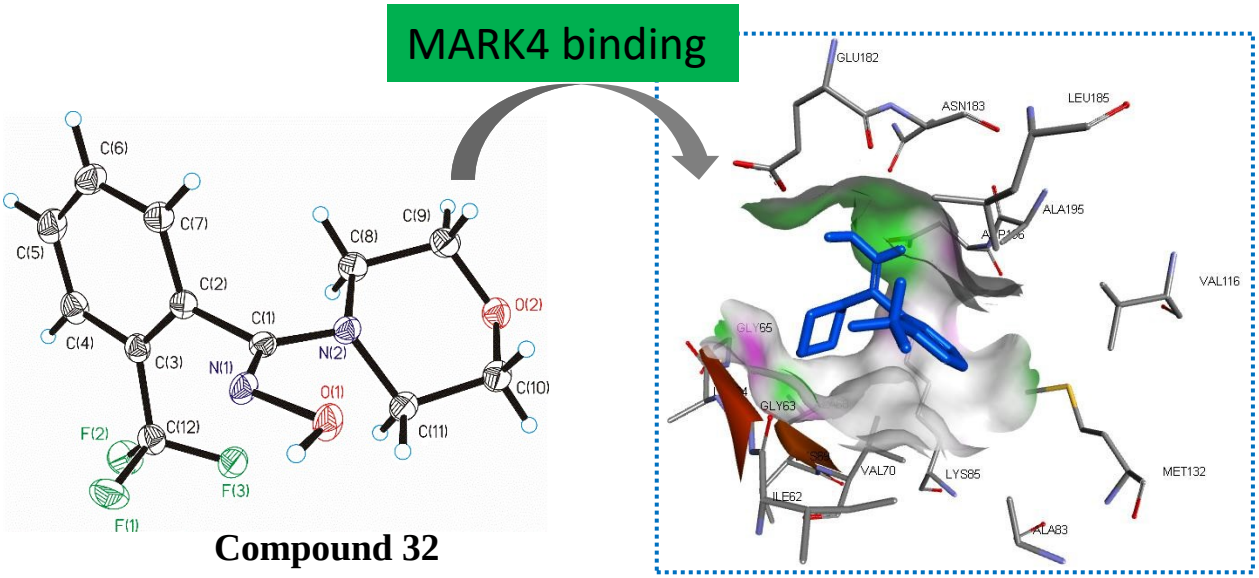

Compound 32

Interaction of compound 32 with various active site residues of MARK4